Effect of Broaching Machining Parameters, Residual Stresses and Cold Work on Fatigue Life of Ni-based Turbine Disk P/M Alloy at 650°C

J. Telesman[1], T.P. Gabb[1], P.T. Kantzos[2] and L.J. Ghosn[1]

[1] NASA Glenn Research Center, Cleveland, OH, USA

[2] Honeywell Aerospace, Phoenix, AZ, USA

Abstract

Machining parameters can influence fatigue life by altering residual stresses, cold work and surface roughness. A study was performed to examine the effect of various broaching machining parameters on high temperature fatigue lives of a nickel-based disk alloy. The influence of tool wear and broaching speed were studied and their effect on residual stresses, cold work and surface roughness was quantified. These variables were shown to have a substantial effect on fatigue lives, the failure mode type and location. The relationships between these parameters and fatigue crack initiation mechanisms are detailed. Statistical analyses evaluating these relationships are presented.

Keywords

Broaching; tool wear; tool speed; fatigue; superalloys; residual stress; cold work; surface roughness; inclusions

1. **Introduction**

Nickel-based superalloys provide a unique set of high temperature, high strength mechanical properties which make them well suited for use in gas turbine engines. However, this same set of excellent mechanical properties makes them susceptible to surface damage induced by various manufacturing steps used to produce turbine disk components. It has been recognized that machining processes-induced surface flaws can compromise the integrity of these highly loaded components by causing premature crack initiations and high cycle fatigue failures (1-4). Such events have led to uncontained disk failures (5).

The machining anomalies can affect the surface integrity of the components by creation of flaws such as surface tearing, inclusion cracking, cavity formation, carbide cracking or grain pullouts (1, 6, 7). Aggressive machining conditions have also been shown to induce local changes in the microstructure by creating what is known as a “white layer” consisting of nano-scale grain structures (6, 7, 8). This reduced ductility layer has been shown to severely reduce the fatigue life under high temperature, high stress conditions (1, 5, 8). Further, machining grooves, deep scratches and other artifacts create localized stress concentrations which also can induce early crack initiation (9, 10).

One of the most challenging geometries in machining of turbine components are the fir tree slots in the disk rim regions used to insert and structurally support turbine blades. These are highly loaded, highest temperature sections of the disks which are susceptible to fatigue, creep and environmental damage. The blade attachment locations are considered to be fracture critical to the integrity of the engine. Due to their complex geometries, a highly specialized broaching process is typically employed to machine-in the fir tree attachment features. Due to the high strength of the disk superalloys, the cutting edges of the broaching tools can wear down quickly as a function of parameters such as broaching speed, cutting force and lubrication (10, 11). This can result in smearing of the surface layer and changes in the surface roughness (1, 12). The material deformation occurring during the broaching process is referred throughout the manuscript as cold work even though the machining process does significantly increase the local temperatures. However, as will be shown later, large amounts of material deformation remain signifying that no significant recovery process has taken place.

Only a limited amount of research has been published regarding the effect of broaching process parameters on fatigue lives of disk superalloys. Chen et al (13) compared fatigue behavior of Inconel 718 tested at room temperature for broached versus as-polished specimens. They showed that without thermal exposures, the fatigue lives of the broached specimens were somewhat longer than that of the as-polished specimens. However, an application of 650°C/300h thermal exposure treatment prior to testing decreased the broaching-induced surface compressive stresses and resulted in reversal of this behavior with the as-polished specimens producing longer fatigue lives. They also showed that a change of crack initiation location from surface to sub-surface increased fatigue life. They concluded that the relaxation of near-surface compressive residual stresses is detrimental to fatigue life. Others have also pointed to the importance of the machining-induced residual stresses on fatigue life (1, 6, 14, 15)

Connolley et al. (16) studied the effect of broaching process on 600°C fatigue behavior also in Inconel 718. They found that the broaching process which led to more severe subsurface deformation produced the biggest fatigue life debit. Fatigue lives were affected by surface roughness, with the final polishing step having a beneficial effect on fatigue lives.

In order to increase the understanding of the effect of broaching process on fatigue lives, this paper examines in detail the effect of various broaching parameters on high temperature fatigue lives of a NASA developed nickel-based Low Solvus High Refractory (LSHR) powder metallurgy disk alloy (17). The influence of tool wear and broaching speed are examined in terms of their effect on fatigue lives. The role that residual stresses, cold work and surface roughness have on fatigue lives was also evaluated. The relationship between these parameters and fatigue crack initiation mechanisms are detailed. Finally, a statistical model linking these parameters to fatigue life is presented.

2. **Materials and Experimental Procedures**

A powder metallurgy LSHR disk superalloy having the composition (in weight percent) 3.5Al–0.019B–0.045C–20.3Co–12.15Cr–0.09Mn–2.7Mo–1.5Nb–1.2Ta–3.5Ti–0.1V–3.85W–0.05Zr-bal. Ni was tested in this study. Powder was produced using argon gas atomization, screened to 53 µm (- 270 mesh), consolidated by hot isostatic pressing, and extruded. Cylinders machined from the extrusion were isothermally forged to produce pancake forgings about 23 cm in diameter and 3.8 cm in height. Each disk was subsolvus solution heat treated in a furnace at 1135 °C for 1.5 h, then fan air cooled. It was subsequently aged by a two-step process consisting of 855 °C for 4 h followed by 775 °C for 8 h. This yielded the microstructure shown in Figure 1 with linear intercept grain size of 4.2 µm measured from etched metallographically prepared sections per ASTM E112-13. Secondary γ' particles were about 0.088 ± 0.024 µm (mean ± standard deviation) in equivalent radius, and tertiary γ' particles were 0.0160 ± 0.0036 µm in radius, also shown in Figure 1. Four tensile tests performed at 650 °C per ASTM E21-20 indicated the material had a tensile yield strength at 0.2 % offset of 1091 ± 48 MPa (mean ± standard deviation), ultimate tensile strength of 1483 ± 34 MPa, elongation of 17.2 ± 2.4 %, and reduction in area of 23.2 ± 4.1 %. Further details of these measurements are provided in (18).

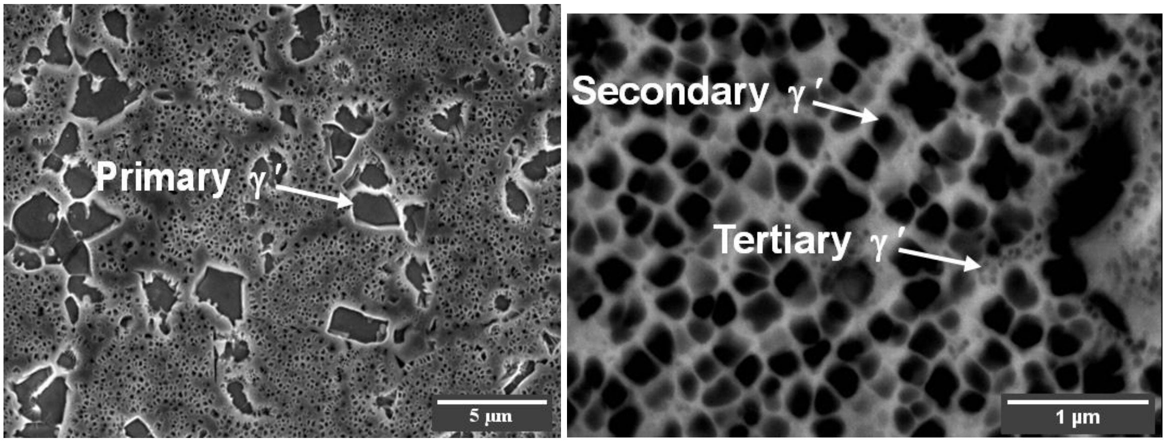

Figure 1. Typical microstructure of the tested subsolvus LSHR disk superalloy.

Segments of the heat-treated pancake forgings approximately 100 mm in length, 37 mm in width and 28 mm in thickness were electro-discharge machined (EDM) out of the pancake forgings. Each segment was broached on two sides of the blanks by Honeywell Aerospace using their production tooling, lubrication oil, to produce a double edge notch (DEN) specimen geometry, Figure 2a. Next, each broached disk forging segment was sectioned by EDM in the longitudinal direction into five separate specimens of approximately 5 mm in thickness, Figure 2b. Finally, the width of each double edge broached specimen was trimmed to achieve a width of 25.4 mm, per Figure 2c so that the specimen dimensions would be compatible with the wedge load testing machine fixtures. All surfaces, with the exception of the broached notches, were finished through low stress grinding. Sharp corners of the broached notches adjacent to the specimen faces were chamfered to reduce the known additional stress concentrations at these corners.

a) b) c)

Figure 2. a) Full thickness broach segment; b) segment sectioned length-wise into four pieces; c; each segment trimmed and machined into fatigue specimens used for testing. Note that in the study the full thickness broached segments were sectioned to produce five fatigue specimens.

The two broaching variables evaluated were broaching speed and tool sharpness. The three broaching speeds studied were termed “slow”, “medium” and “fast”. Variation in speed studied was much greater than is used in actual practice, with the “fast” condition exceeding production allowable limits. The “sharp” condition reflected specimens broached after re-sharpening of the broaching cutting tools, while the “dull” condition exceeded the allowable number of broached runs in a production setting. Thus, six broaching conditions were studied through the combination of these two broaching process variables.

Since residual stresses are known (1, 6, 14, 15) to have a significant effect on fatigue behavior, an extensive study of residual stress profiles created by the different broaching conditions was performed using x-ray diffraction. Both residual stress measurements and the corresponding cold work were determined using the full thickness broached forging segments for each of the six broach conditions evaluated. In order to allow for the x-ray beam to reach the regions of interest without being blocked by the fir tree features, an EDM sectioning was performed approximately 2.5 mm above the root of the notch as shown in Figure 3a. After gaining access to the region of interest, surface residual stress measurements were made along three rows of the broached notch at intervals of approximately 2.5 mm from the tool entry into the slot, Figure 3b. Thus, thirty surface residual stress measurements were made for each of the six blanks representing the various broaching conditions studied. Based on the initial surface residual stress readings, two locations along the broached slot were selected for measurement of the residual stress and cold work profiles in the depth direction. Measurements of the residual stresses and cold work were performed by Lambda Technologies of Cincinnati, Ohio. The (311) reflection of Mn radiation was used for the measurements. To obtain residual stress depth profiles, surface layers were carefully electropolished away with the change in residual stresses caused by material removal accounted for by a standard process developed by Lambda Technologies (19). The percent cold work was determined from the breadth at half height of the (311) diffraction peak using the full-width, half-maximum method from data obtained for residual stress measurements. The empirical relationship for cold work versus peak breadth was established using specimens deformed to known levels of true plastic strain.

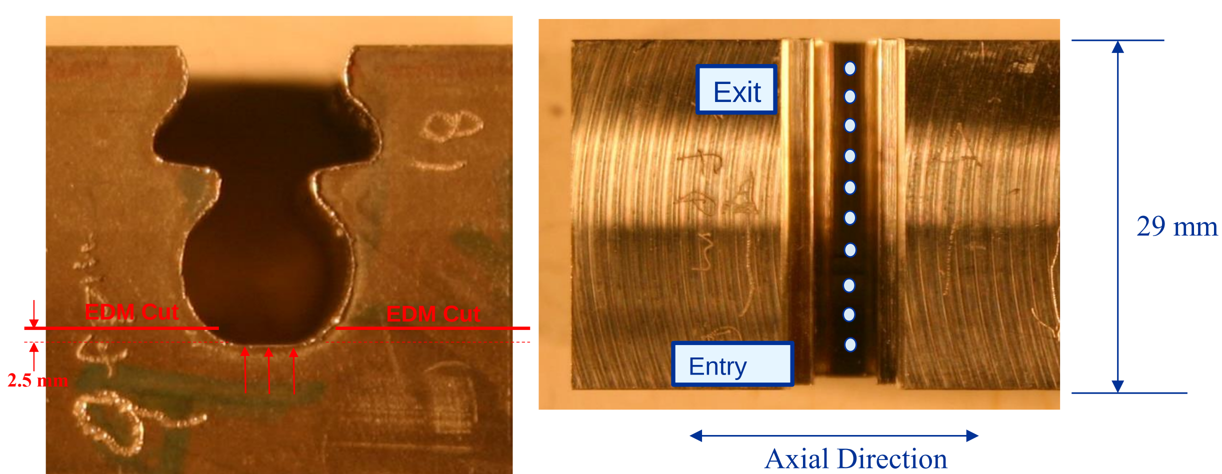

a) b)

Figure 3. a) Sectioning of the full thickness broached segment for x-ray diffraction measurements. Three rows of measurements taken as indicated by the arrows; b) locations along the broached slot for surface residual stress measurements. For simplicity only one of the three rows is shown in the schematic.

Fatigue testing was conducted on the broached DEN configured specimens at 650°C utilizing a furnace designed for this specimen geometry. The maximum applied net section stress was 965 MPa with the tests conducted at a stress ratio R=0.05 and a test frequency of 0.333 Hz. At least four test repeats were performed for each broaching condition studied.

As part of the broached surface characterization process, surface profilometry was performed to quantify the surface roughness for each tested specimen prior to initiation of mechanical testing. The surface roughness analysis was performed using an Alicona Infinite Focus 3D Microscope. The surface roughness was quantified by the use of three different roughness parameters, R_a, R_q and R_z where R_a is the arithmetic average roughness, R_q is the root mean square or geometric roughness and R_z is the difference between the highest and the lowest value of the peaks scanned (20).

3. **Results**

3.1 Finite Element Analysis

A 3D finite element elasto-plastic analysis (FEA) was performed for the DEN specimen geometry in terms of both von Mises and loading direction stresses. Tabular true-stress/true-strain data was used for this analysis based on actual tensile tests performed at 650 °C assuming the isotropic hardening feature in ABAQUS software. The effect of creep was ignored for this analysis. The analysis was done at both maximum and minimum applied loads, Figure 4. The elastic stress concentration (K_t) of the DEN specimen was calculated to be approximately 1.6. As shown in Figure 4, in the loading direction the highest stresses are slightly below the surface. Due to notch plasticity, substantial compressive stresses form on unloading. The FEA analysis shown in the figure was done only for the first loading cycle.

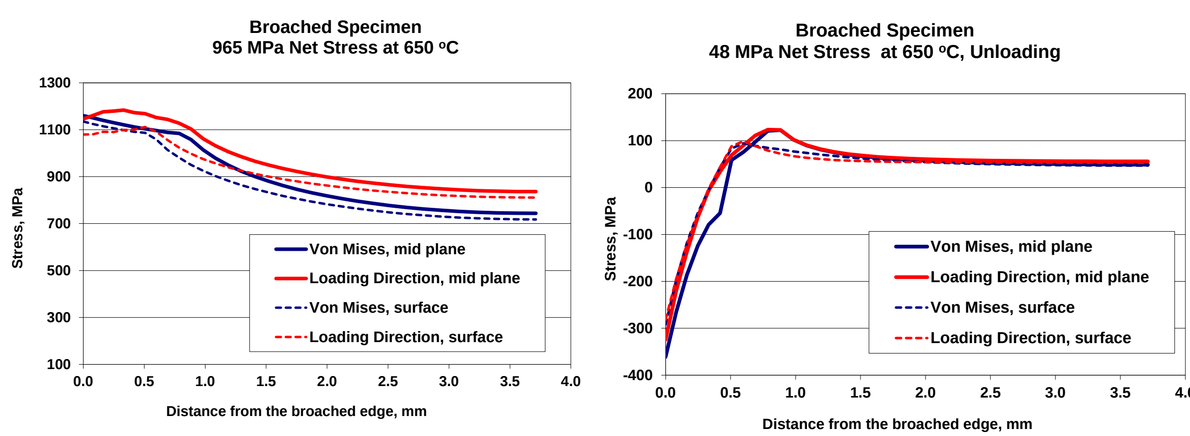

a) b)

Figure 4. Elasto-plastic FEM analysis of the concentrated stresses as function of the distance from the notch; a) at maximum applied stress; b) after unloading at minimum applied stress.

3.2 Surface Roughness Analysis

The comparison of the surface roughness parameters for the six different broaching conditions evaluated is shown in Table I. The roughness measurements were normalized to allow for an easier comparison of the surface roughness parameters. The highest surface roughness was measured for the “sharp” condition subjected to a “slow” cutting speed. However, the relative differences in the surface roughness parameters for the “sharp” tooling for all three speeds were within 10% of the highest values. In the case of the “dull” tooling, the differences in the surface roughness between “slow” and “medium” were relatively small with the “slow” condition exhibiting the rougher surface finish. In contrast, the “fast” cutting speed for the “dull” tooling produced a large reduction in surface roughness with that condition exhibiting the lowest surface roughness of all six conditions evaluated.

Table I. Normalized Surface Roughness – Three Parameters

Speed	Sharp			Dull		
	Ra	Rq	Rz	Ra	Rq	Rz
Slow	1	1	1	0.77	0.83	0.99
Medium	0.88	0.90	0.92	0.75	0.72	0.82
Fast	0.90	0.93	0.96	0.45	0.50	0.66

3.3 Residual Stresses and Cold Work

Surface residual stress profiles generated as a function of the distance from the slot entry of the broaching cutting tool are shown in Figures 5a and 5b for “sharp” and “dull” tooling respectively. The surface residual stress values were measured every 2.5 mm along the length of the broach slot. The data is shown for all three broaching speeds evaluated. As seen in both figures, the surface residual stresses are not uniform across the broach slots. The highest measured stresses are in the regions near the tool entry point for both sets of tooling at all broaching speeds evaluated. However, there are significant differences in terms of the magnitude and the range of residual stresses both as a function of tool wear, broaching speed and the distance along the slot from the entry of the broaching tool. Calculated +/- standard deviation of each residual stress measurement varied with stress magnitude, ranging from +/- 13 MPa at a measured stress of -14 MPa to +/- 48 MPa at a measured stress of -1649 MPa.

In the near tool entry region “sharp” tooling produced mostly tensile residual stresses, Figure 5a. Surface residual stresses in the magnitude of +345 MPa or higher were measured up to a distance of 7.5 mm from the tool entry for both the “high” and the “medium” broach speeds. After reaching that distance, the residual stresses decreased gradually as a function of the distance from tool entry. Near the tool exit point, for the two higher speeds the residual stresses were close to zero. The “low” speed tensile residual stresses for “sharp” tooling were considerably lower. They were close to zero near the tool entry point and became compressive after a distance of 7.5 mm. The magnitude of the compressive stresses approached -345 MPa at a broach slot distance of 12.5 mm, after which the residual stresses became less compressive as a function of distance to the tool exit point.

In contrast, for the “dull” tooling only the “high” broaching speed resulted in tensile residual stresses in the broaching tool entry region, Figure 5b. For the other two speeds the residual stresses near tool entry were close to zero. After 5 to 7.5 mm, all three broaching speeds resulted in a steep increase in the magnitude of compressive residual stresses up to a distance of approximately 12.5 mm, after which all the compressive residual stresses plateaued and continued at these compressive values up to the tool exit. “High” broaching speed produced the least compressive residual stresses with a maximum compressive stress of about -700 MPa. The “low” speed “dull” tooling conditions produced the highest compressive residual stresses of about - 1000 MPa. As is also clear from the comparison of the “sharp” to “dull” surface residual stresses, the “dull” tooling resulted in significantly larger changes of residual stresses when examined in terms of the distance along the broaching slots.

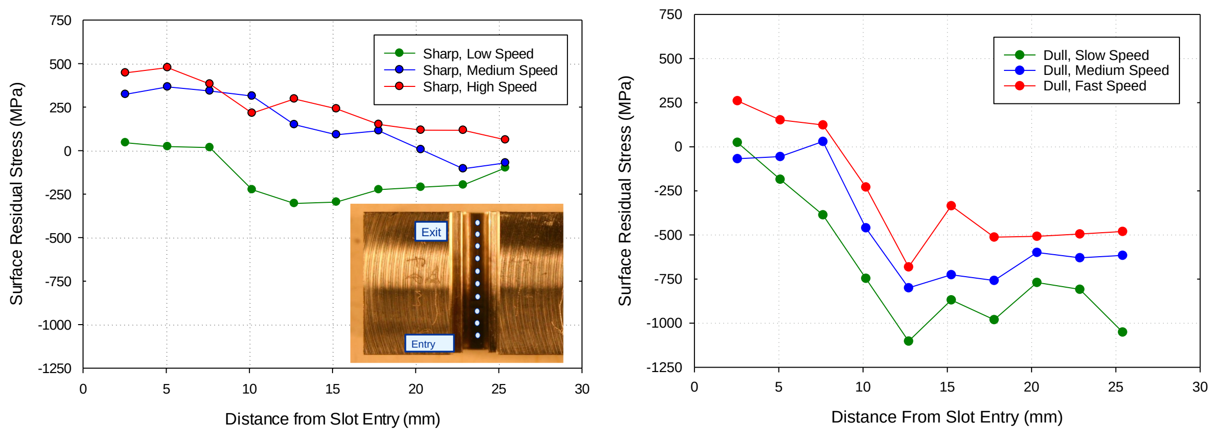

a) b)

Figure 5. Surface residual stresses along the length of the broaching slot; a) “sharp” tooling; b) “dull” tooling.

Based upon the surface residual stress readings along the broaching slots, two locations were selected to perform residual stress measurement depth profiles. The two locations were 5 mm from the tooling entry point and 20.3 mm from the entry point and thus near to the exit point, per Figure 3. The measurements were taken at 12 µm depth increments until such depths where residual stresses approached zero. As shown in the Figures 6a and 6b, the depth and the magnitude of the residual stresses were considerably different for the “dull” versus “sharp” tooling. The depth of compressive residual stresses was approximately 125 µm for the “dull” condition regardless of the broaching speed or the slot location. At the 5 mm location, two of the three “dull” cutting speeds exhibited surface tensile residual stresses which very quickly became highly compressive and then gradually decreased in the amount of compression until the residual stresses disappeared at approximately 125 µm. At the 20.3 mm location, for all three speeds the “dull” tooling exhibited compressive residual stresses with the magnitude of the compressive stresses being largest for the “slow” broaching speed.

The measured residual stresses were very different for the “sharp” tooling. The depth of the residual stresses was much shallower extending only to approximately 25-30 µm at both 5mm and 20.3 mm broach slot locations for all three broaching speeds. Furthermore, a majority of these residual stresses were primarily tensile, with the exception of “slow” speed which did exhibit some surface compressive stresses, Figure 6.

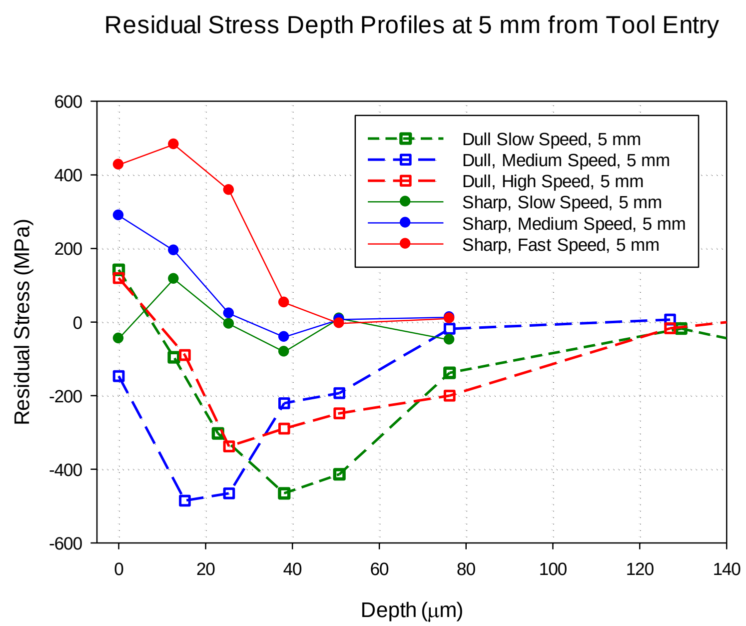

a)

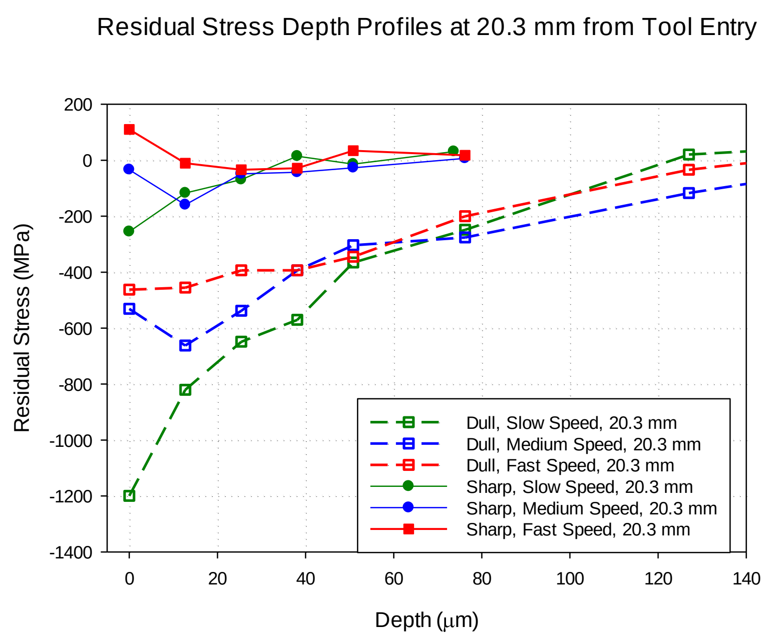

b)

Figure 6. Residual depth profiles at respective distances of 5 mm (a) and 20.3 mm (b) along the broaching slot taken from the entry point of the broaching tool.

Figure 7 shows the calculated surface cold work as a function of distance from the broaching tool entry point. While there appears to be considerable scatter among the measured values, the following trends were noted. The “dull” tooling produced a higher amount of cold work than “sharp” tooling. For “dull” tooling the cold work appeared to stay relatively uniform along the slot length. For the “sharp” tooling conditions, the highest measured amount of cold work was near the broach tool entry location which then decreased with the distance from entry. In the areas beyond the broaching tool entry regions, the "dull" conditions produced 30-40% cold work while the "sharp" tooling resulted in 15-25% cold work. Due to the data scatter, no clearly observed trends were detected in terms of the effect of broaching speed on the amount of measured cold work for either tool wear category, Figure 7.

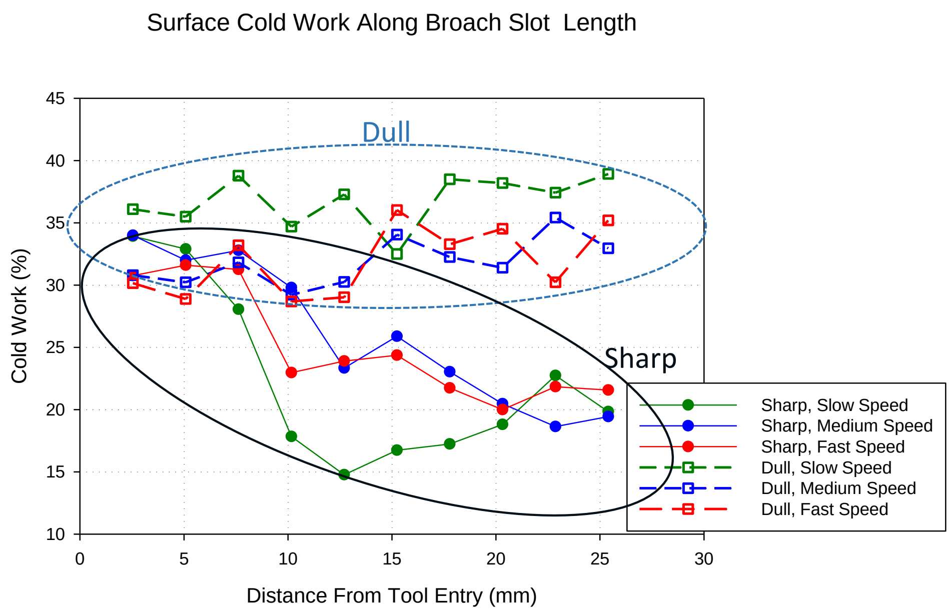

Figure 7. Surface cold work for all six broaching conditions measured as a function of distance from the broaching tool entry point.

3.4 Fatigue Results

The fatigue results of the tests conducted in the program are shown in Table II. Each DEN specimen tested is identified based on the tooling wear condition, broach speed, fatigue life and failure location. The same data set of fatigue lives is shown in Figure 8a in terms of a cumulative failure probability plot. A probability scale is the inverse of the Gaussian distribution function where the sigmoidally shaped cumulative distribution function plotted on a probability scale is a straight line. As shown, fatigue testing resulted in over two orders of magnitude spread in fatigue lives ranging from 15,840 cycles to 1.75×10^6 for the specimens which were all tested under the same test conditions. The mean life based on all accumulated fatigue tests was 219,641 cycles with a standard deviation of 324,018 cycles. Separating the fatigue results by tool wear, the calculated mean and standard deviation of the fatigue lives are shown in Figure 8b. The data reveals that the mean life of the "dull" broached specimens was almost 2x greater than the mean fatigue life of the specimens machined using sharp tooling. However, as seen in Figure 8b, the slope of the "dull" cumulative failure probability data set is shallower than that of the "sharp" set indicating a greater amount of scatter in fatigue lives.

Table II. Broached Specimen Fatigue Test Results

Specimen ID	Tool Wear	Broach Speed	Fatigue Life (cycles)	Failure Location
0A-B2-E	Sharp	Slow	85,489	Subsurface
9C-B2-A	Sharp	Slow	223,199	Subsurface
9C-B2-B	Sharp	Slow	102,267	Surface
9C-B2-C	Sharp	Slow	201,055	Surface
9C-B2-D	Sharp	Slow	1,139,688	Subsurface
9C-B2-E	Sharp	Slow	117,507	Subsurface
9D-B1-A	Sharp	Slow	118,743	Subsurface
9D-B1-B	Sharp	Slow	223,513	Subsurface
0A-B1-A	Sharp	Medium	135,254	Subsurface
0A-B1-D	Sharp	Medium	47,742	Surface
9B-B1-B	Sharp	Medium	20,175	Surface
9B-B2-B	Sharp	Medium	102,636	Subsurface
9B-B2-E	Sharp	Medium	32,963	Subsurface
9D-B7-C	Sharp	Medium	36,832	Surface
9D-B7-E	Sharp	Medium	34,457	Subsurface
0A-B3-A	Sharp	Fast	270,052	Subsurface
9C-B3-A	Sharp	Fast	24,741	Surface
9C-B3-B	Sharp	Fast	109,303	Subsurface
9C-B3-C	Sharp	Fast	58,473	Subsurface
9C-B3-D	Sharp	Fast	56,467	Surface
9C-B3-E	Sharp	Fast	37,698	Surface
9D-B2-D	Sharp	Fast	183,025	Subsurface
0AB5-1-B	Dull	Slow	122,281	Subsurface
0FB6-1-A	Dull	Slow	1,756,765	Subsurface
9BB4-1-A	Dull	Slow	15,840	Surface
9BB4-1-B	Dull	Slow	228,766	Subsurface
9BB4-1-C	Dull	Slow	136,366	Subsurface
9DB6-1-B	Dull	Slow	261,560	Subsurface
9DB6-1-D	Dull	Slow	562,636	Subsurface
0AB6-1-D	Dull	Medium	133,207	Subsurface
0FB4-1-A	Dull	Medium	121,170	Subsurface
9BB5-1-A	Dull	Medium	304,561	Subsurface
9BB5-1-B	Dull	Medium	103,160	Subsurface
9BB5-1-C	Dull	Medium	174,581	Subsurface
9BB5-1-D	Dull	Medium	556,377	Subsurface
9CB6-1-E	Dull	Medium	627,471	Subsurface
9DB4-1-C	Dull	Medium	26,914	Surface
9BB6-1-A	Dull	Fast	158,799	Subsurface
9BB6-1-C	Dull	Fast	271,302	Subsurface
0FB5-1-B	Dull	Fast	22,606	Lost
9DB5-1-A	Dull	Fast	59,640	Surface

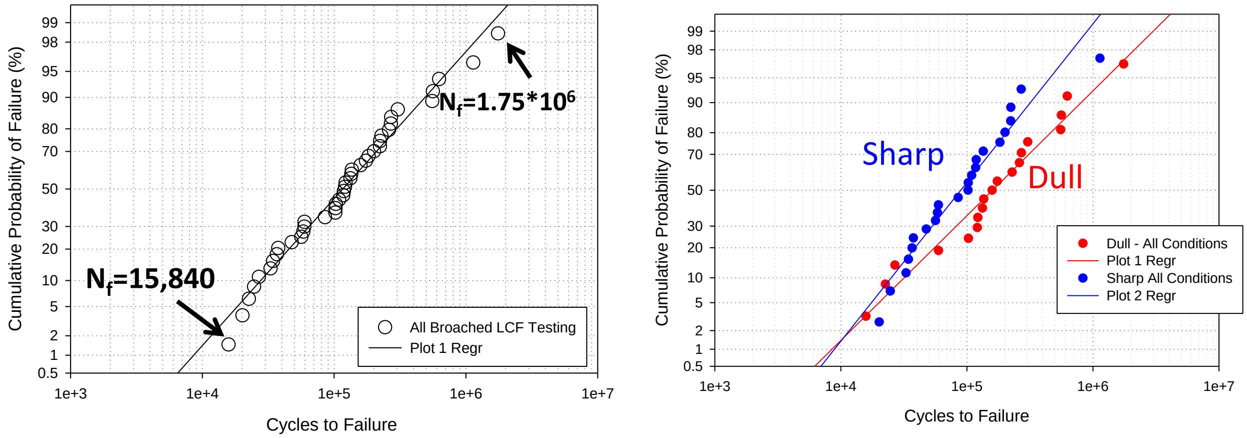

a) b)

Figure 8. a) Cumulative probability of failure plots for all fatigue tests performed; b) the fatigue data separated into "sharp" and "dull" sets.

The effect of broaching speed and tool wear on fatigue life are shown in Table III as a function of the mean, standard deviation and the maximum and minimum fatigue lives for each of the six conditions evaluated. All the fatigue results will be discussed in more detail in the next section.

Table III. Statistical Characterization of Fatigue Results for all Six Broaching Conditions

Tool Wear	Broach Speed	Mean	Std Dev	Min Life (cycles)	Max Life (cycles)
Sharp	Slow	276,433	353,239	85,489	1,139,688
Sharp	Medium	58,580	43,057	20,175	135,254
Sharp	Fast	105,680	90,219	24,741	270,052
Dull	Slow	440,602	581,658	15,840	1,756,765
Dull	Medium	255,930	222,422	26,914	627,471
Dull	Fast	128,087	111,453	22,606	271,302

4. Discussion

4.1 Residual Stresses

The results indicate a strong relationship between the measured residual stresses and cold work with the broaching parameters examined. One of the most intriguing findings is a significant change in the measured surface residual stresses for the "dull" tooling set as a function of the distance along the broaching slot from the entry point of the broaching tool, Figure 5. These differences in the measured residual stresses may be caused by a change in the coefficient of friction from the initial entry point for the "dull" tooling which may need more energy to initiate the cutting process than to continue it. As will be discussed later on, this lack of uniformity of residual stresses along the length of the broaching slot was likely the major contributor to the large scatter in the fatigue lives of the "dull" tool set specimens.

Microstructural Near-Surface Deformation

A comparison of the effect of different broaching parameters on near-surface microstructural deformation is shown in Figure 9. Some deformation damage is visible for all shown conditions. The grains were deformed in the broaching direction. In some of the surface-intersecting grains, deformation resulted in slip band formation. However, none of the broaching conditions were severe enough to produce the white etch layer which can cause very early fatigue crack initiation (1, 5, 8).

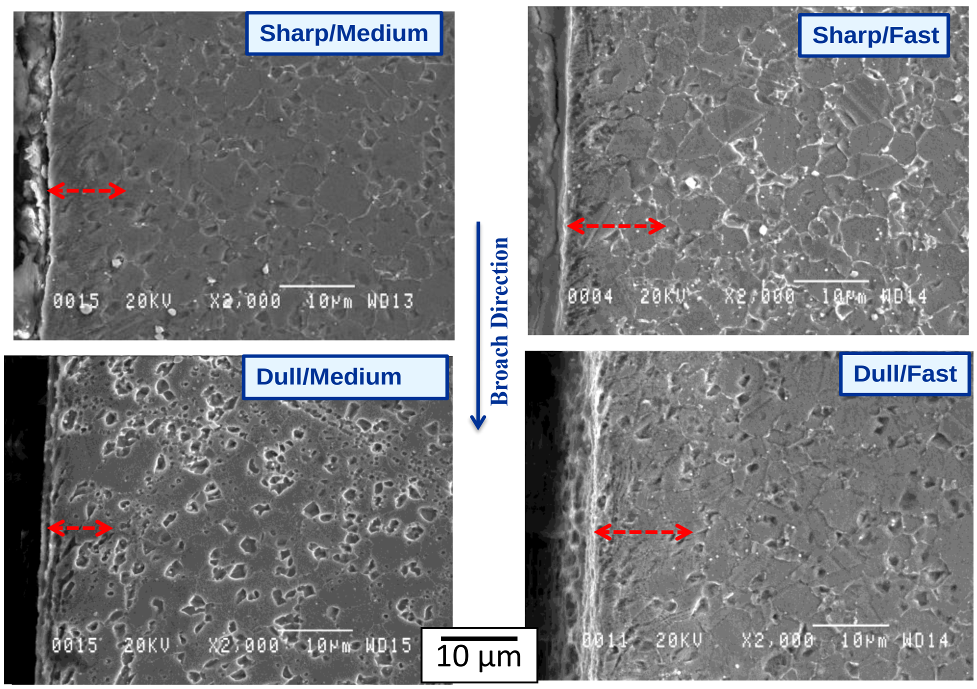

Figure 9. Comparison of the visible microstructural deformation imparted by the broaching process for four different tool wear/broach speed parameter combinations.

As shown in Figure 9, the depth of the visibly deformed microstructural region was similar for both “sharp” and “dull” tool wear conditions and appeared to be more dependent on the broaching speed than tool wear. However, even the deeper of the two deformed regions, “fast” speed at (10-15 µm), was still much shallower in depth than the 125 µm residual stresses determined by x-ray diffraction, Figure 6. Thus, the visible deformed layer is not a reliable indicator of the extent of the depth of the residual stresses.

As was shown in Figure 7, for the “dull” tool wear condition, cold work was measured to be approximately in the 30 to 40% range with the maximum compressive residual stresses in the order of -700 MPa while the residual stress depth approached 125 µm. These levels of cold work and residual stress depth approach those found after an application of shot peening for this class of disk superalloys (21). For disk alloys shot peened using typical peening conditions, the surface cold work is in the 30-50% range, the depth of the compressive residual stresses is in 150-200 µm range while the maximum compressive residual stresses are -960 to -1170 MPa. The main difference is that shot peening aims to produce uniform compressive stresses over the entire peened surface, while the “dull” broaching process resulted in a large range of residual stress responses depending on the location along the broached slot, as was shown in Figure 5. Yet, as will be discussed later in more detail, in the broached fatigue specimens the crack initiation observations reveal the importance of the residual stresses in a manner similar to shot peening.

4.2 Failure Modes and Locations

Fractography was performed on the tested DEN fatigue specimens. As was shown in Table II, both surface and subsurface failures were observed. For both "sharp" and "dull" conditions most failures occurred from subsurface locations with 64% of the former and 83% of the latter exhibiting subsurface failures. All the internal crack initiations occurred at small ceramic inclusions which are inherent to this class of superalloys. Most of these crack-initiating inclusions were alumina with few other cracks initiating from zirconia inclusions, Figure 10. In contrast, the majority of the surface initiation sites were broaching machining grooves, Figure 11. These surface cracks not only initiated at these grooves but also tended to grow for some distance along these grooves. A few other surface initiations occurred at locations showing no obvious surface features.

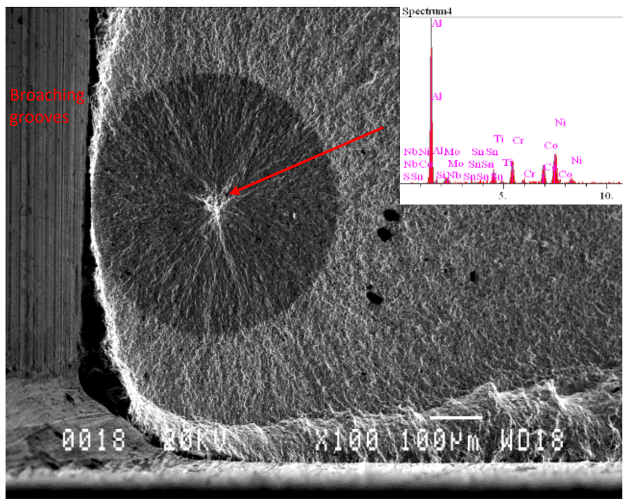

Figure 10. Typical subsurface crack initiation occurring at an alumina inclusion (inset)

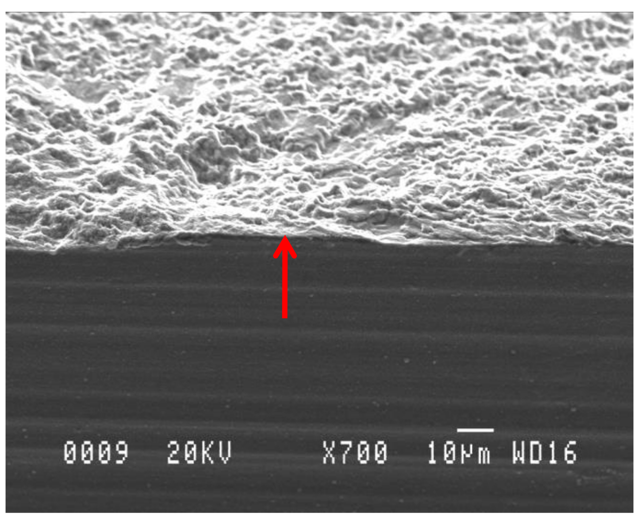

Figure 11. Typical surface initiation with the crack initiating and propagating in the early stages from a broaching groove.

The failure initiation location (internal vs. surface) had a significant effect on the fatigue life. The fatigue life data from Figure 8a is replotted in Figure 12 so that the cumulative failure probability plot includes the location of the crack initiation site. As shown, the surface failures for both “dull” and “sharp” conditions, marked by open symbols with circular dots, not only tended to produce some of the lowest fatigue lives, but also exhibited similar fatigue lives. In contrast, the subsurface initiations resulted in longer lives for both conditions, with the “dull” condition resulting in 2x greater mean fatigue lives than the “sharp” tooling.

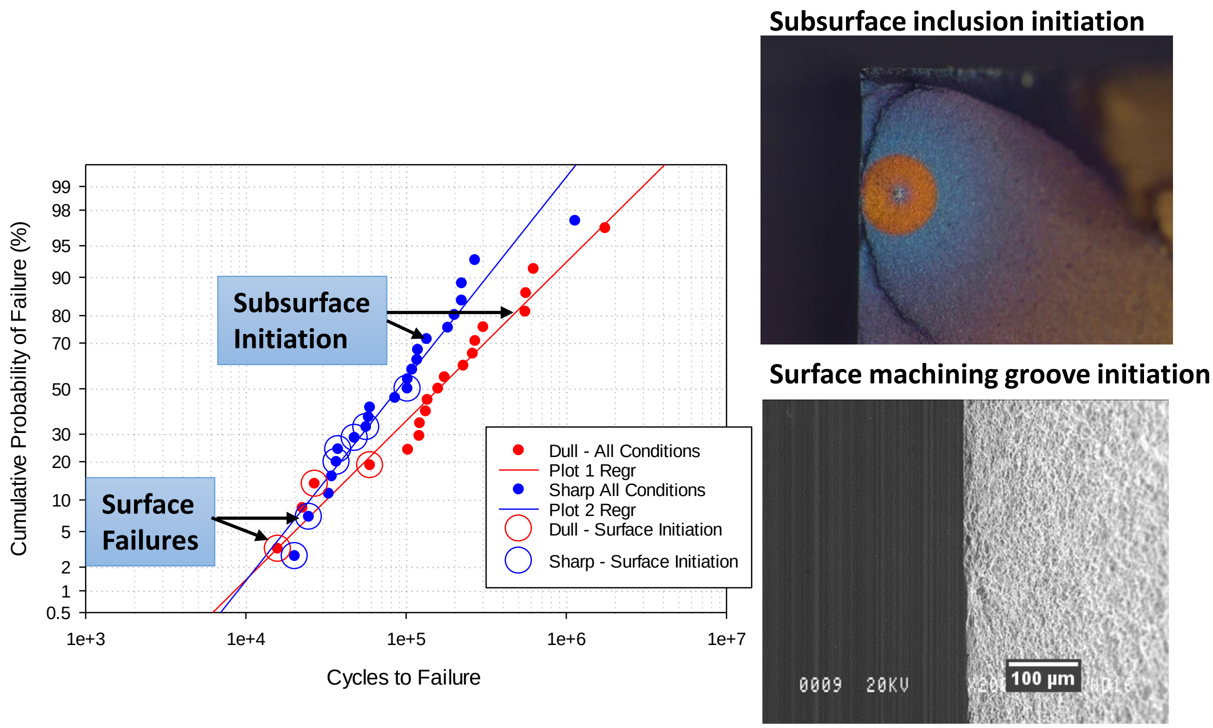

Figure 12. Cumulative probability of failure plot separating surface initiations from subsurface for both tool wear conditions.

To examine the observed trends for subsurface initiations in more detail, the fatigue data in the form of the cumulative probability failure plot is shown in Figure 13a for internal initiations for both tool wear conditions. As observed in this figure, the failure lives of the internally-initiated “dull” specimens are substantially longer than those of the internal failures for the “sharp” tooling condition specimens. Figure 13b, reveals that the distribution of the distances from the initiation site to notch surface depended on the tool wear condition with the “sharp” tooling initiation sites being grouped together, mostly within 200 µm of the surface. In comparison, the “dull” tooling resulted in a wide scatter of the internal crack initiation locations with most of them being scattered within 600 µm of the surface.

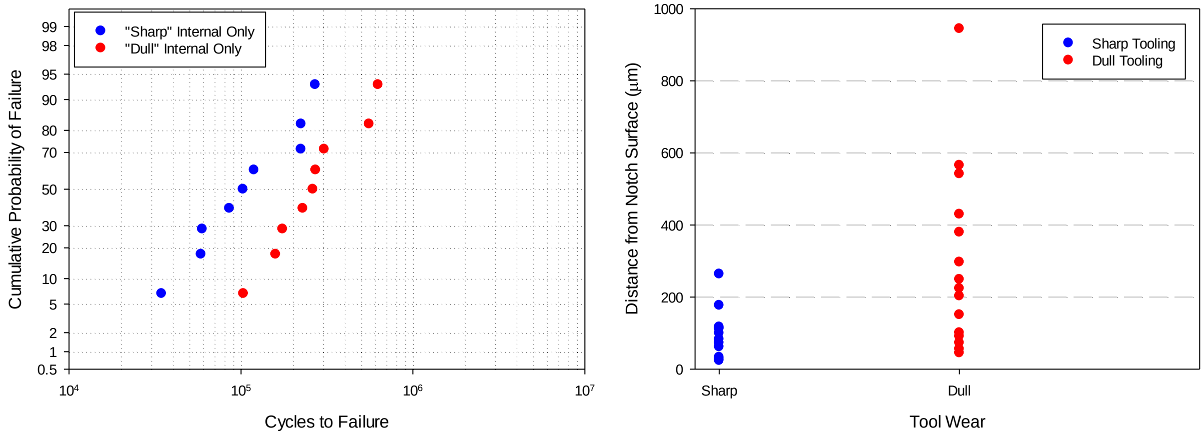

a) b)

Figure 13. a) Cumulative probability of failure for internal initiations as a function of tool wear for all three broaching speeds; b) Distance of the subsurface initiations to the notch surface as a function of tool wear.

Since all these subsurface fatigue crack initiations occurred from inclusions and not from machining-induced surface flaws or localized surface stress concentration features, it is reasonable to assume that the broaching machining process did not physically cause the crack initiation events. However, the location and distribution of the residual stresses created by broaching appears to correlate closely with the observed subsurface crack initiation events. As was shown in Figures 6a and 6b, the magnitude and the depth of the residual stresses formed by the “sharp” tooling is shallower than the “dull” tooling for all three speeds which can explain the preference for crack initiation events occurring very near the surface since the applied mechanical stresses in the surface region are not significantly affected by the residual stresses. This also explains the larger percentage of actual surface initiations observed for specimens produced using “sharp” tooling. A previous study (22) of an inclusion-seeded superalloy also noted similar influence of residual stress distributions on the location of fatigue initiation sites.

In contrast, for the “dull” tooling broached specimens, Figure 6b, the presence of higher magnitude and greater depth of the compressive residual stresses can retard crack initiation and propagation occurring from the near-surface inclusions. These residual stress states produced by dull tooling result in the crack initiation events taking place at inclusions present farther away from the surface and slowing down the FCG propagation rates as the crack has to grow through the near-surface compressive stresses which increases the fatigue lives. However, due to the large variability of the residual stresses for the “dull” tooling as a function of distance from the broach tool entry position, Figure 5, there is a large scatter both in the location of the fatigue initiation sites and the corresponding fatigue lives since some of the fatigue specimens are likely to represent broach regions where the residual compressive stresses are relatively low.

The trends of the fatigue lives and crack initiation locations observed in this study are similar to those observed in other studies which examined the effect of the residual stresses induced by shot peening, specimen machining or other surface enhancement methods (21, 22). All these studies pointed to the importance of residual stresses in controlling crack initiation and the subsequent small fatigue crack propagation rates. Another contributing factor favoring internal initiations in these notched fatigue specimen geometries is the shift of the highest maximum tensile stresses away from the notch surface as was determined by the elasto-plastic FEM analysis shown in Figure 4.

4.3 Effect of Broaching Speed on Fatigue Behavior

The examination of the effect of broaching speed on fatigue lives further clarifies the role that the residual stresses have on fatigue behavior for both tool wear conditions. The cumulative probability failure plots for “sharp” tooling at each broaching speed are shown in Figure 14 together with an inset of the previously shown surface residual stresses for each individual broach speed. As shown in the inset graph, the surface residual stresses for the “low” speed exhibited much higher compressive residual stresses than those for the “medium” and “fast” conditions. The cumulative probability failure plot shows that the mean fatigue life for the “low” speed condition was considerably longer than for the other two speeds.

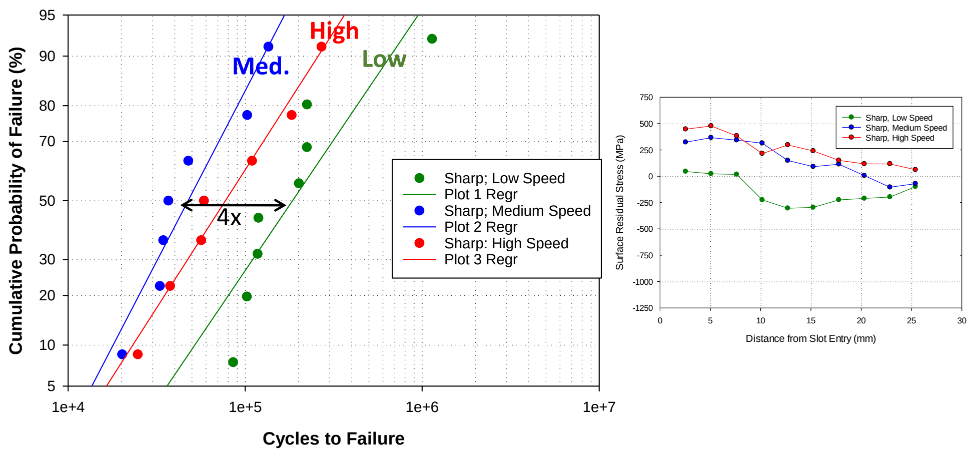

Figure 14. Effect of broaching speed on fatigue lives for “sharp” tooling and the accompanying surface residual stresses shown in the inset.

A similar cumulative probability plot is shown in Figure 15 for the “dull” tooling together with the inset of the measured surface residual stresses at the three broaching speeds. While the “slow” speed did produce the most compressive surface residual stresses overall, the magnitude of the differences in the residual stresses between the three speeds was often smaller than for the “sharp” tool set. Consequently, there was a much lower spread in the mean fatigue life (2x) for the three speeds for the “dull” set in comparison to the “sharp” set (4x). The “slow” speed still produced the highest mean fatigue life, however it should be noted that the “dull” tooling with the “slow” speed produced the largest difference in fatigue lives for the individual tests of any of the conditions evaluated. Thus, the highest life of 1.75×10^6 cycles and the lowest fatigue life of 15,840 cycles were both measured within the “slow” speed “dull” tooling specimen set. The large range in the measured surface residual stresses for this condition may have been responsible for this occurrence, since the region near the tool entry point measured near zero residual stresses while in other regions the surface stresses reached -1000 MPa.

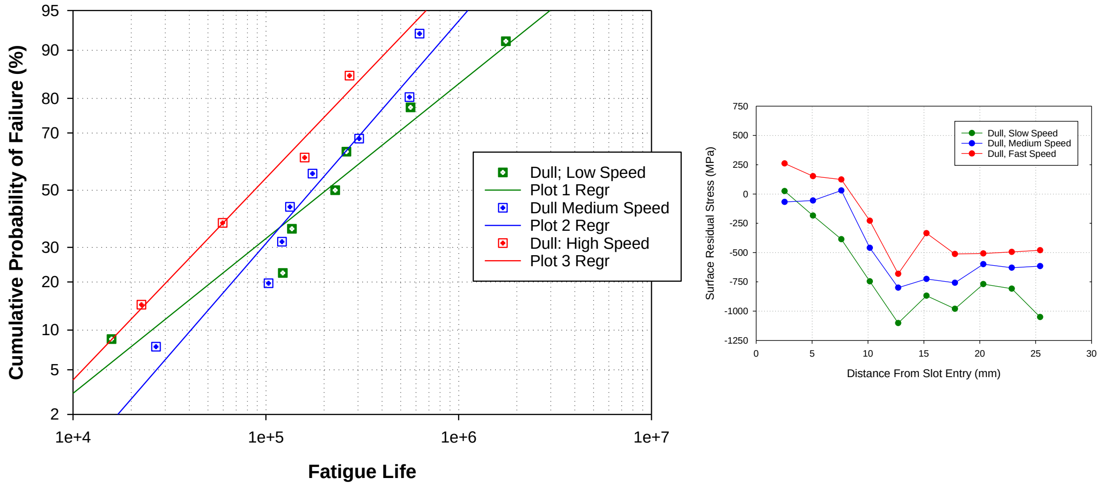

Figure 15. Effect of broaching speed on fatigue lives for "dull" tooling and the accompanying surface residual stresses shown in the inset.

4.4 Surface Finish

As was shown in Table I, the differences in the measured surface finish for the three broaching speeds of the specimens machined using "sharp" tooling were very limited, with the "slow" speed exhibiting approximately 10% higher surface roughness parameters values than the other two speeds evaluated. Thus, these results proved to be of limited value in evaluating the importance of the surface finish on fatigue life. In contrast, for the "dull" tooling the "fast" broaching speed resulted in a reduction of approximately 40% in the surface roughness in comparison to the "slow" broaching speed. This decrease in the surface roughness for the "fast" speed condition did not translate into an improvement in the fatigue lives in comparison to the "slow" speed condition, Figure 15. In fact, the "fast" speed condition resulted in the mean fatigue being approximately 2x lower than for the "slow" broaching speed.

The reduction in fatigue lives for the "fast" broaching speed condition does not indicate that the local increase in stress concentration provided by surface machining grooves has no effect on fatigue lives. As was already pointed out in Figure 11, a majority of surface-initiated fatigue failures occurred at the machining grooves which have both a higher local stress concentrations as well as higher local deformed regions. Instead, the higher residual compressive stresses for the "slow" condition shifted the failure initiation sites to subsurface regions thus reducing the influence of the higher surface stress concentration of the grooved regions on fatigue lives.

Three different surface roughness measurement parameters were evaluated, Table I. However, the small differences in the relative magnitude of these measured parameters were inadequate to conclude which of these parameters is best suited to characterize the surface finish of broached specimens.

4.5 Statistical Analyses

The magnitude of the mean fatigue lives is not the only important life property to be considered when evaluating the effect of various broaching conditions on component durability. In the previously discussed results, it was apparent that the magnitude and the depth of the compressive residual stresses have a profound effect on LCF lives. However, for both engine designers and their customers the reliability of the turbine components is of even greater importance. The reliability calculations not only consider the magnitude of the mean lives but also have to take into consideration the scatter of fatigue lives in order to obtain statistically meaningful measures of reliability.

Multi-variate statistical regression analyses were performed to assess statistical relationships between the broaching conditions and the resulting residual stresses, cold work, fatigue life and data scatter.

The analysis was performed using the JMP®version 11 statistical software package. Since the broaching tools were used only at two levels of wear, as in freshly re-sharpened and at the worn level specified for this re-sharpening, these wear levels were assigned values of -1 and 1, respectively. Since broaching tool speed was consistently set at evenly spaced intervals to produce low, medium, and high speeds, these speed levels were assigned values of -1, 0, and 1. So in this way broaching tool wear and speed were represented in standardized form *V′* as defined using equation 1:

$$V' = ((V-V_{mid}))/(0.5*(V_{max}-V_{min})) \qquad (1)$$

In equation (1), for each independent variable, V is the actual value measured for a specimen, V_{max} is the maximum value measured across all specimens, V_{min} is the minimum value measured across all specimens, and $V_{mid} = (V_{max} + V_{min})/2$. This produced a range of values from –1 to +1 for each of the independent broaching variables of sharpness and speed. The “scaled” expressions using these standardized variables *V′* are useful for analyzing derived relationships, as the relative effect of each significant variable on the response can be assessed in the regression equation by directly comparing the magnitude of the coefficient for each variable. Regression equations were derived by comparing the results of both forward and reverse stepwise selection of terms, with a 90 % probability of significance required for inclusion of a term. The coefficient of determination (R^2) and the coefficient of determination with adjustment for the number of predictive variables (R^2_{adj}) were used as indications for an equation’s goodness of fit. The regression analyses were intended to consistently screen for and compare derived relationships between broaching conditions, residual stress, cold work, and fatigue lives.

The effect of broaching variables on the mean residual stress and standard deviation (StDev) of residual stress are shown in Figure 16, while the effect that these variables have on mean cold work and the StDev of cold work are depicted in Figure 17. The goodness of fit as indicated by the coefficients of determination for each derived regression equation was high, indicating these were useful relationships. As shown by the statistical fitting expression in Figure 16a, the magnitude of the mean compressive residual stresses increases with increased tool wear, i.e., “dull” tooling, and with a decrease in broaching speed. As revealed by the values of the coefficients in the regression equation of Figure 16a, the increase in the tool wear was a greater contributor to the compressive residual stresses than tool speed. Figure 16b shows that the StdDev of residual stresses increased with increasing wear (i.e. more variability with “dull” vs. “sharp” tooling), while stepwise selection of the regression equation indicated that speed did not have a significant influence These quantitative results agree with trends presented in Figure 5 which, as discussed earlier, pointed to greater mean compressive stresses for the “dull” tooling and also smaller differences in the measured surface residual stresses for the “sharp” tooling as a function of the distance along the broaching slot for all broaching speeds evaluated.

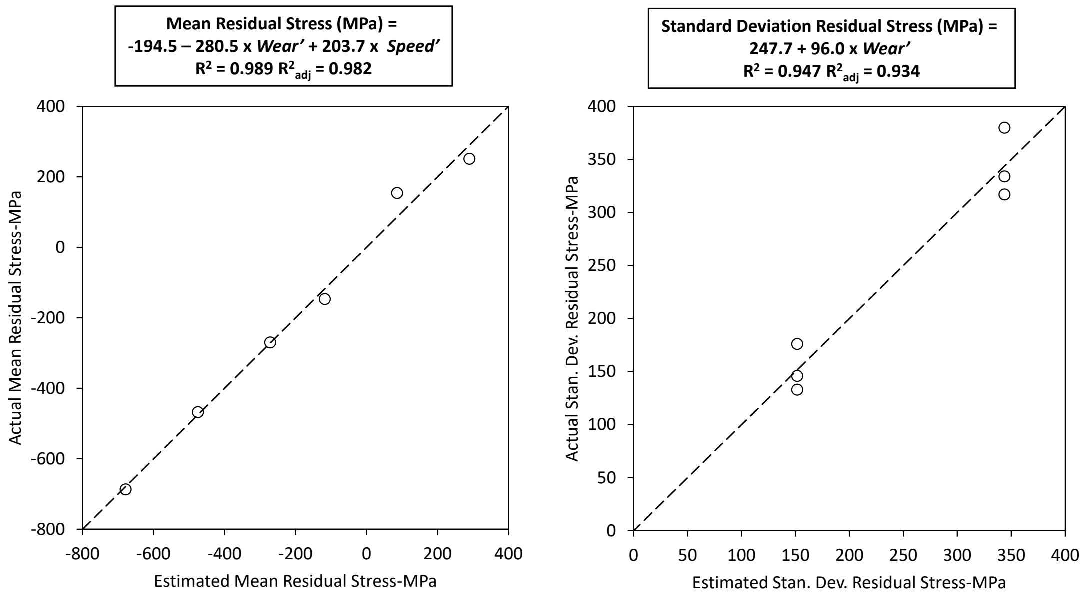

a) b)

Figure 16.a) Mean Residual Stress magnitude became more compressive with increased tool wear followed by decrease in tool speed; b) StdDev of Residual Stress decreased with decreasing tool wear.

The multi-variate statistical relationships between the broaching parameters and the measured surface cold work and its StdDev are shown in Figures 17a and b respectively. As observed, the regression fits are in agreement with trends observed in Figure 7, showing that "sharp" tooling decreases mean cold work, especially at low speed. Further, as depicted in Figure 17b, StdDev of cold work decreases with increasing wear, especially at low speed. The adjusted R^2 values for equations are equal or greater than 0.90 indicating high goodness of fit.

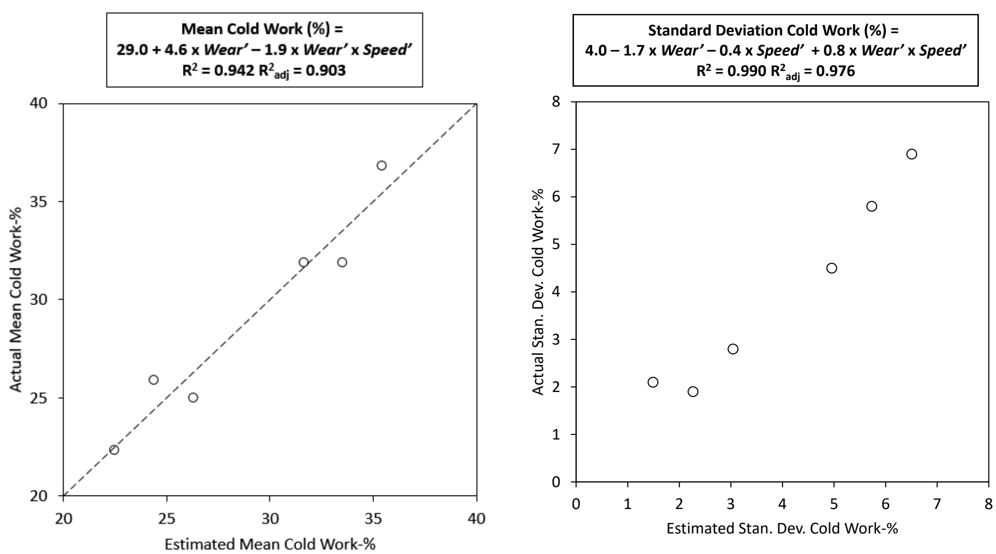

a) b)

Figure 17. a) Mean Cold Work decreases with decreasing tool wear, especially at low speed; b) StDev of Cold Work decreases with increasing tool wear, especially at low speed.

The influence that the mean residual stresses and mean cold work have on Mean Log Life and its StDev of Log Life is shown in Figures 18a and 18b respectively. The predicted expression in Figure 18a was determined using actual mean residual stress and mean cold work values and resulted in an adjusted R^2 of 0.76. The analysis was also performed using scaled variables (*V'*) of mean residual stress and mean cold work, to produce scaled coefficients in order to determine which of the variables has a more pronounced influence on Mean Log Life. The results are shown in the Scaled Estimates table in Figure 18a. As shown, the value of the coefficient of the magnitude of compressive residual stress, approximately -0.50, is almost twice that of the mean cold work, approximately -0.29. Thus, the influence of the residual stress is greater than that of the cold work. Therefore, not surprisingly, the lower standard deviation of residual stress also correlated with lower StDev of Mean Log Life, Figure 18b.

Mean Log Life =
5.99967 – 0.00106 x Mean Residual Stress – 0.03973 x Mean Cold Work
R^2 = 0.857 R^2_{adj} = 0.761

Term	Scaled Estimate
Intercept	5.05663
Mean Residual Stress'	-0.49496
Mean Cold Work'	-0.28805

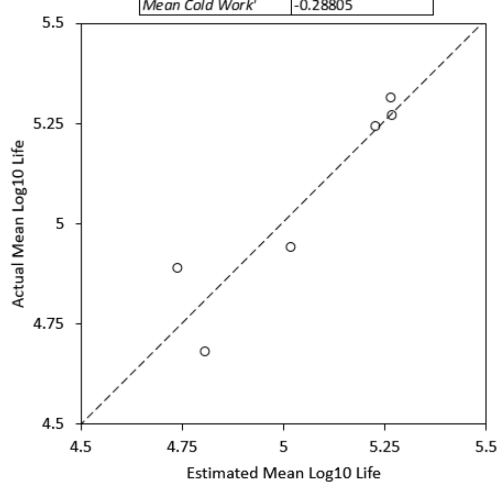

a)

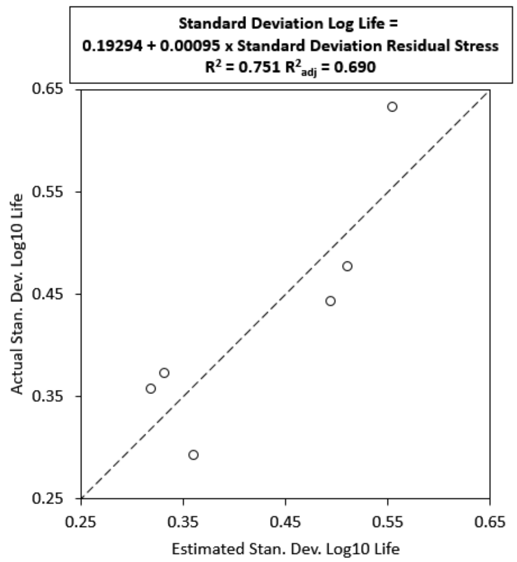

b)

Figure 18; a) Mean Log Life increased most strongly with higher compressive residual stress, then decreasing mean cold work; b) smaller standard deviation of residual stress correlated with lower StDev of Log Life.

The multi-variate analysis was also performed in an attempt to link Log Life of each individual test with tool wear and broaching speed parameters. According to the analysis, low tool wear and low speed correlated with the longest Log Life. However, due to the significant overlap of fatigue lives and extensive data scatter for the different broaching variables examined as was shown in Figures 8, 14 and 15, the resulting adjusted R^2 of 0.12 indicates poor fit, Figure 19a. Mean Log Life observed for each broaching condition was correlated only as a function of broaching speed, the resulting expression showing that low speed produced the longest Mean Log Life, Figure 19b, although still with a poor fit. This low goodness of fit could be largely attributed to varied response at the “medium” speed. The inability to predict the fatigue life with high goodness of fit is not surprising since, as was shown earlier, the mean fatigue life was greater for the “dull” tooling yet at the same time “sharp” tooling produces the smallest scatter in life, Figure 19c.

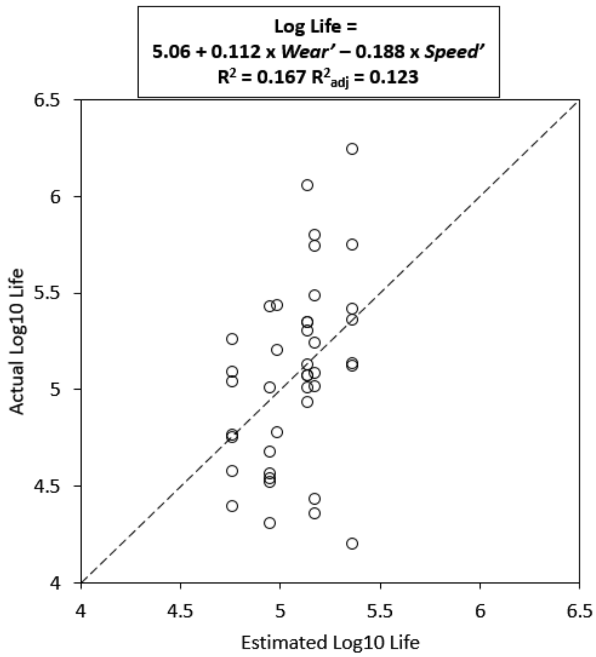

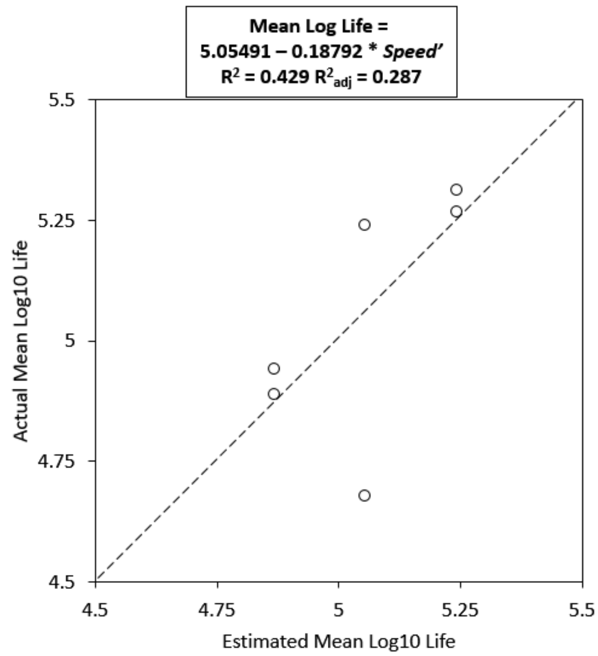

a) b)

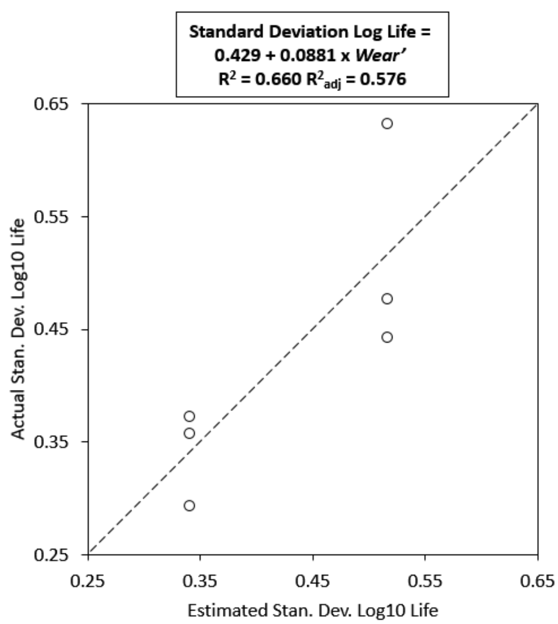

c)

Figure 19: a) "Sharp" tool wear and low tool speed correlate with the longest Log Life, but at very low goodness of fit; b) Mean Log10 Life at each broaching condition correlated to low tool speed also at a low goodness of fit; c) "Sharp" tooling results in the lowest StdDev of Log10 Life.

The magnitude of the scatter in fatigue lives encountered for the "dull" machined specimens overwhelms the increase in the mean fatigue lives. The best example of this phenomena are the seven tests performed on the "dull" specimens machined using "slow" speed. As shown in Tables II and III, this particular set resulted in both the lowest and highest fatigue lives which varied by over two orders of magnitude. The calculated standard deviation of the fatigue lives for this set was approximately 30% greater than its mean fatigue life, Table III. While the fatigue life scatter for the “sharp” tooling specimens is lower than for the “dull” tooling, the magnitude of the scatter is still large, thus the attempts to predict the fatigue life in terms of the tool wear and tool speed parameters produced regressions with low goodness of fit.

This inability of deriving statistical expressions with high goodness of fit for Log Fatigue Life in terms of broaching parameters needs to be contrasted with well correlated relationship between Mean Log Fatigue Life and the magnitude of residual stresses and cold work shown in Figure 18a. Further, very strong relationships between the broaching parameters and residual stress and cold work were also established, Figures 16 and 17. However, the large scatter of residual stresses and cold work as a function of the location along the broaching slot from the tool entry point precluded the possibility of deriving strong relationships between the broaching parameters and fatigue life. Multiple fatigue specimens had been machined across each broached slot as shown in Fig. 2, producing scatter in residual stress and cold work among the specimens for each broaching condition.

The results illustrate the need for reliable and uniform residual stresses and cold work to be present in the fir tree regions of the turbine disks so that fatigue life limits and turbine durability can be established with much higher degree of confidence. The common practice by the engine companies of shot peening these regions after the broaching process is completed (23) helps with establishing more uniform residual stress fields across these highly loaded features.

The present study evaluated the effect of broaching parameters on fatigue life under rather limited testing conditions due to the need for multiple test repeats. Due to the importance of residual stresses and cold work on LCF lives of broached regions, more research is required to establish how the demanding in-service conditions affect these variables as a function of prolonged high temperature exposures and the applied complex load histories. These studies should also include the evaluation of the post-machining shot peening process on fatigue behavior.

5. Conclusions

A study of broaching machining parameters was conducted to determine their effect on fatigue lives of a Ni-based turbine disk alloy. The two main broaching parameters evaluated were tool wear and broaching speed. The fatigue results were evaluated in terms of the measured residual stresses, cold work and surface roughness parameters. The main conclusions from the results of this study are as follows:

1) The measured surface residual stresses were significantly different for the “dull” tooling versus “sharp” tooling, with the increase in tool wear corresponding to higher compressive residual stresses. Also, the decrease in the broaching speed resulted in a higher magnitude of compressive stresses for both “sharp” and “dull” tooling.

2) While the surface residual stresses were fairly uniform across the entire broaching slot for the “sharp” tooling, the behavior was very different for “dull” tooling. For the latter, the magnitude of the compressive residual stresses increased substantially as a function of the distance from the entry point of the broaching tool along the length of the broached slot.

3) The residual depth profiles for the “dull” tool set were substantially more compressive than the “sharp” tool set. Further, the depth of the residual stresses was considerably deeper for the “dull” set than for the “sharp” tooling.

4) The measured surface cold work was significantly higher for the “dull” tooling in comparison to the “sharp” tooling even though there was a significant data scatter for both tool wear conditions.

5) “Sharp” tooling produced higher surface roughness which did not vary significantly for the three broaching speeds evaluated. For the “dull” tooling, the lowest surface roughness was produced by the highest broaching speed. However, the changes in the surface roughness did not correlate to the fatigue lives.

5) The mean fatigue life of the “dull” tool set was approximately 2x greater than for the “sharp” tooling. However, the scatter in the fatigue lives was greater for the “dull” tooling. The slowest broaching speeds tended to produce the longest fatigue lives within each of the tool wear condition data sets.

6) For both tool wear conditions a majority of the crack initiation sites occurred in the subsurface regions with the cracks initiating at small ceramic inclusions. The “dull” tooling produced a higher percentage of these internal initiations which also tended to be located at greater depths from the surface than the comparable inclusion initiations occurring for the “sharp” tool set. The failures which initiated at the notch surfaces mostly started at the broach machining grooves.

7) Multi-variate statistical expressions were derived to quantify the relationships between broaching conditions evaluated and the residual stress, cold work and fatigue lives. The relationships between the broaching parameters and residual stress and cold work were determined with high goodness of fit. The effect of the residual stresses and cold work on fatigue life was also shown to be of high importance. Yet, due to the large scatter in the fatigue lives, only a poor (not statistically significant) relationship between the fatigue lives and the broaching parameters was identified. The large scatter in the fatigue lives was likely caused by the lack of uniformity of the residual stresses across the machined broached slots.

Acknowledgements

The work was performed under the auspices of the NASA’s Aeronautics Rotary Wing Program.

References

1) R. M’Saoubi, J.C. Outeiro, H. Chandrasekaran, O.W. Dillon Jr, I.S. Jawahir, A review of surface integrity in machining and its impact on functional performance and life of machined products, Int. J. Sustain. Manuf., 1, 2008, 203–236.

2) D. Taylor and M. Clancy, The Fatigue Performance of Machined Surfaces, Fatigue Fract. Engng. Mater. Struct., Vol 14, No. 2/3, 1991, 329-336.

3) Qi Huang and Jing Xin Ren, Surface integrity and its effects on the fatigue life of the nickel-based superalloy GH33A, Int. J. Fatigue, 13, No 4, 1991, 322-326.

4) Z. Liao, A. la Monaca, J. Murray, A. Speidel, D. Ushmaev, A. Clare, D. Axinte, R. M'Saoubi, Surface integrity in metal machining - Part I: Fundamentals of surface characteristics and formation mechanisms, International Journal of Machine Tools and Manufacture, 2021.

5) M.C. Hardy, C.R.J. Herbert, J. Kwong, W. Li, D.A. Axinte, A.R.C. Sharman, A. Encinas-Oropesa and P.J. Withers, Characterising the Integrity of Machined Surfaces in a Powder Nickel Alloy used in Aircraft Engines, 2nd CIRP 2nd CIRP Conference on Surface Integrity, Procedia CIRP 13, 2014, 411–416.

6) A.R.C. Sharman , J.I. Hughes, K. Ridgway, An analysis of the residual stresses generated in Inconel 718TM when turning, Journal of Materials Processing Technology 173, 2006, 359-367.

7) A. Chamanfar, H. Monajati, A. Rosenbaum, M. Jahazi, A. Bonakdar, E. Morin, Microstructure and mechanical properties of surface and subsurface layers in broached and shot-peened Inconel-718 gas turbine disc fir-trees, Materials Characterization 132, 2017, 53-68.

8) A.M. Wusatowska-Sarnek, B. Dubiel, A. Czyrska-Filemonowicz, P.R. Bhowal, N. Ben Salah, and J.E. Klemberg-Sapieha, Microstructural Characterization of the White Etching Layer in Nickel-Based Superalloy, Met Trans A, Vol 42A, 2011, 3814-3825.

9) C.R.J. Herbert, D. A. Axinte, M.C. Hardy, P. D. Brown, Investigation into the characteristics of white layers produced in a nickel-based superalloy from drilling operations, 1st CIRP Conference on Surface Integrity, Procedia Engineering 19, 2011, 138–143.

10) Q. Bonnardel, V. Wagner, G. Dessein, V. Dutilh, Sebastien Mandrile, Effects of cutting parameters over turning of UDIMET® 720 superalloy in a broaching process simulation, 16th CIRP Conference on Modelling of Machining Operations, Procedia CIRP 58, 2017, 572 – 577.

11) X. Kong, B. Li, Z. Jin and W. Geng, Broaching Performance of Superalloy GH4169 Based on FEM, J. Mater. Sci. Technol., 27, 2011, 1178-1184.

12) X. Liang, Z. Liu, B. Wang, State-of-the-art of surface integrity induced by tool wear effects in machining process of titanium and nickel alloys: A review, Measurement, 132, 2019, 150-181.

13) Zhe Chen, J.Moverare, R.L. Peng , S. Johansson, D. Gustafsson, On the conjoint influence of broaching and heat treatment on bending fatigue behavior of Inconel 718; Materials Science & Engineering A, 671, 2016, 158-169.

14) P. Prevey and W. Koster, Effect of Surface Integrity on Fatigue of Structural Alloys at Elevated Temperatures, in *Fatigue at Elevated Temperatures*, ed. A. Carden, A. McEvily, and C. Wells (West Conshohocken, PA: ASTM International, 1973), 522-531.

15) S. M. Afazov & A. A. Becker & T. H. Hyde, Effects of micro-stresses from machining and shot-peening processes on fatigue life, Int. J. Adv. Manuf. Technol., 51, 2010, 711–722.

16) T. Connelley, M.J. Starnik, and P.A.S. Reed, Effect of Broaching on High-Temperature Fatigue Behavior in Notched Specimens of INCONEL 718, Met Trans, Vol. 35A, 2004.

17) T.P. Gabb, J. Gayda, J. Telesman and P. Kantzos, Thermal and mechanical property characterization of the advanced disk alloy LSHR, NASA TM-2005-213645, NASA, 2005.

18) T.P. Gabb, J. Gayda, J. Telesman, L.J. Ghosn, A. Garg, Factors Influencing Dwell Fatigue Life in Notches of a Powder Metallurgy Superalloy, Int. J. of Fatigue, 48, 2013, 55–67.

19) P.S. Prevey, X-ray diffraction residual techniques, Metals Handbook. 9th ed: American Society for Metals, Metals Park, OH; 1986, 80–392.

20) C. Maheswara Rao, K.Venkatasubbaiah and K. Jagadeeswara Rao, Experimental Investigation of Surface Roughness Characteristics Ra, Rq and Rz; International Journal of Hybrid Information Technology, 9, No.7, 2016, 373-388.

21) P. Prevey, J. Telesman, T. Gabb and P. Kantzos, FOD Resistance and Fatigue Crack Arrest in Low Plasticity Burnished IN718, Proceedings: 5th National Turbine Engine High Cycle Fatigue Conference Chandler, AZ, March 7-9, 2000.

22) J. Telesman, T.P. Gabb, P.T. Kantzos, P.J. Bonacuse, R.L. Barrie, C.A. Kantzos, Effect of a large population of seeded alumina inclusions on crack initiation and small crack fatigue crack growth in Udimet 720 nickel-base disk superalloy, Int. J. of Fatigue, 142, 2021.

23) D. Grieving, M. Gorelik, H. Kington, in: D.O. Thompson, D.E. Chimenti (Eds.), Manufacturing Related Residual Stresses and Turbine Disk Life Prediction, Review of Quantitative Nondestructive Evaluation, Vol. 24, American Institute of Physics, Melville, NY, 2005, 1339–1346.